

Cite this: *RSC Adv.*, 2019, 9, 11567

# Biocompatible carbon-doped MoSe<sub>2</sub> nanoparticles as a highly efficient targeted agent for human renal cell carcinoma

Li Gao,<sup>a</sup> Yi-zeng Fan,<sup>b</sup> Tao-hong Zhang,<sup>a</sup> Hui-qiu Xu,<sup>a</sup> Xian-ling Zeng,<sup>a</sup> Tao Hou,<sup>b</sup> Wei-chao Dan,<sup>b</sup> Jin Zeng<sup>\*b</sup> and Rui-fang An<sup>†a</sup>

MoSe<sub>2</sub> is a typical transition-metal dichalcogenide material, and many researches have been focused on using its property of near infrared strong absorption for laser mediated photothermal cancer treatment. However, the anti-cancer effect of MoSe<sub>2</sub> and its possible mechanism in renal cell carcinoma (RCC) is still unclear. RCC has high incidence of metastasis, which is known as one of the most lethal malignancies in the urological system. This study revealed that the carbon-doped MoSe<sub>2</sub> particles can obviously inhibit proliferation for 786-O and ACHN cells. Meanwhile, the carbon-doped MoSe<sub>2</sub> nanoparticles have little impact on the viability of KH-2 cells *in vitro*. The mechanism analysis revealed that the carbon-doped MoSe<sub>2</sub> particles have hydrogen bond effect in aqueous solution, and the particle aggregation effect caused the KH-2 cells to have high viability. The carbon-doped MoSe<sub>2</sub> nanoparticles with minimal toxicity may be a potential therapeutic candidate against RCC.

Received 8th February 2019

Accepted 3rd April 2019

DOI: 10.1039/c9ra01029g

rsc.li/rsc-advances

## 1 Introduction

Cancer is a serious threat to human health, and late discovery makes it difficult to cure. So far, early diagnosis is still a major bottleneck to discovering early cancer, and advanced cancer still lacks effective treatment.<sup>1,2</sup> Cancer is easy to cure in the early stage, which is an effective way to improve the cure rate and reduce the mortality of cancer. With the development of modern medicine, researchers have a deeper understanding of the worldwide problem of cancer, and surgery, radiotherapy, chemotherapy and other clinical treatment methods exist. However, all the previously described treatments have certain risks, including killing normal cells, accelerating the metabolism of tumor cells and destroying the immune system. Therefore, it is necessary to find a more effective medicine to improve the cure rate of cancer.

As the third most common urologic malignancy, renal cell carcinoma (RCC) accounts for approximately 3% of all cancers, and 90% of the kidney cancer patients are adults.<sup>3</sup> After treating with advanced diagnostic methods and systemic treatment such as chemotherapy and radiotherapy, patients will have a remarkable improvement in 5 year survival and recurrence-free survival. Despite that, 30% of the kidney cancer patients

continue to progress into the metastatic disease, as a result the median overall survival of metastatic RCC of only 12 months.<sup>4</sup> Furthermore, metastatic RCC is insensitive to chemotherapy, and drugs for immunotherapy and targeted therapy have a low effect.<sup>5</sup> Although targeted drug therapy for RCC has been improved, the response rates of targeted drugs in metastatic RCC remain poor, and the resistance to chemotherapy is a primary obstacle in RCC treatment.<sup>6,7</sup> Thus, it is urgent to explore novel therapeutic agents against RCC.

Now, two-dimensional (2D) layered transition metal dichalcogenides (TMDCs) have drawn great attention as agents for photothermal therapy due to their novel electronic and optical properties.<sup>8–10</sup> The exfoliated TMDCs (MoS<sub>2</sub>, WS<sub>2</sub> and WSe<sub>2</sub>) have lower cytotoxicity than classic 2D materials such as graphene and its analogues.<sup>11</sup> The selenium and molybdenum elements are the necessary trace elements to human body, and the toxicity of MoSe<sub>2</sub> is relatively lower than other two-dimensional transition metal dichalcogenide materials.<sup>12</sup> MoSe<sub>2</sub> is a typical two-dimensional transition metal dichalcogenides material and has always been used in the field of optoelectronics. Furthermore, because of its strong absorption in the near infrared region, MoSe<sub>2</sub> nano materials have been used as photothermal agents for cancer treatment: Zhong *et al.* prepared biocompatible MoSe<sub>2</sub> nanoparticles for efficient targeted photothermal therapy of human lung cancer;<sup>13</sup> Chen *et al.* prepared green nanosheets as a highly efficient photothermal cancer therapy;<sup>14</sup> Pan *et al.* used Gd<sup>3+</sup> doped MoSe<sub>2</sub> nanosheets as a theranostic agent for bimodal imaging and highly efficient photothermal cancer therapy.<sup>12</sup>

<sup>a</sup>Department of Gynaecology and Obstetrics, The First Affiliated Hospital of Xi'an Jiaotong University, Health Science Center, Xi'an Jiaotong University, Xi'an, Shaanxi 710061, P. R. China. E-mail: anrfxjtu@163.com

<sup>b</sup>Department of Urology, The First Affiliated Hospital of Xi'an Jiaotong University, Health Science Center, Xi'an Jiaotong University, Xi'an, Shaanxi 710061, P. R. China. E-mail: zengjin1984@gmail.com

As an inorganic material, normal MoSe<sub>2</sub> has poor suspension property in water condition, and it has poor biocompatibility in tumor therapy. Ultrasonic was used to further process and modify MoSe<sub>2</sub>, and the prepared MoSe<sub>2</sub> materials have good biocompatibility.<sup>15–17</sup> Therefore, it is urgent to find more facile processing strategies for MoSe<sub>2</sub> nano materials formation with excellent biocompatibility and multifunctionality. In this study, ethanol was adopted in the MoSe<sub>2</sub> preparation, and the ultrasonic was used to disperse the MoSe<sub>2</sub> particles in mixture solution (isopropyl alcohol/distilled water). As a result, the prepared MoSe<sub>2</sub> particles contained carbon elements (49.82 wt%) with good biocompatibility. The carbon-doped MoSe<sub>2</sub> nanoparticles have very low toxicity to KH-2 cells, but they can obviously reduce the viability of 786-O and ACHN cells. Despite its potential of anti-proliferation effect, but the carbon-doped MoSe<sub>2</sub> nanoparticles reduced the viability of RCC had not been elucidated clearly. Hence, it is very meaningful to explore the antitumor effect of carbon-doped MoSe<sub>2</sub> nanoparticles on RCC cell lines and to investigate its possible mechanisms.

## 2 Materials and methods

### 2.1 Materials

Selenium (Se) powder was from Beilian Fine Chemicals Development Co., Ltd (Shanghai, China). Sodium molybdate dihydrate (Na<sub>2</sub>MoO<sub>4</sub>·2H<sub>2</sub>O) was bought from Chemical Reagent Plant Four (Tianjing, China). Hydrazine hydrate 80%

(N<sub>2</sub>H<sub>4</sub>·H<sub>2</sub>O) was purchased from Fuyu Fine Chemical Co., Ltd (Tianjing, China). All the materials used in the research were analytic reagent grade (AR).

### 2.2 Cell culture

Human kidney HK-2 cells and human RCC cell lines 786-O and ACHN were obtained from ATCC, and maintained in RPMI-1640 medium (Gibco, USA), containing 10% fetal bovine serum (FBS, Gibco, USA) and 100 U mL<sup>-1</sup> penicillin and 0.1 mg mL<sup>-1</sup> streptomycin (Gibco, USA). The cells were cultured at 37 °C with 5% CO<sub>2</sub> in a humidified atmosphere. The HK-2 cells were immortalized by transduction with human papilloma virus 16 (HPV-16) E6/E7 genes. The cell experiments were carried out in the department of urology, the first affiliated hospital of Xi'an Jiaotong University.

### 2.3 Preparation

The preparation of MoSe<sub>2</sub> nanoparticles: 0.765 g of Na<sub>2</sub>MoO<sub>4</sub>·2H<sub>2</sub>O and 0.5 g of Se powder were dissolved in 40 mL distilled water. Then 20 mL of ethanol and 10 mL of N<sub>2</sub>H<sub>4</sub>·H<sub>2</sub>O were added into the mixture. After stirring for 30 min, the mixture was transferred to a 100 mL Teflon-lined stainless autoclave, which was sealed tightly and maintained at 200 °C for 12 h. Then the reactant was cooled to room temperature naturally. The suspension was centrifuged and washed with distilled water and ethanol for several times. Finally, the product dried at 60 °C to obtain black MoSe<sub>2</sub> powder.

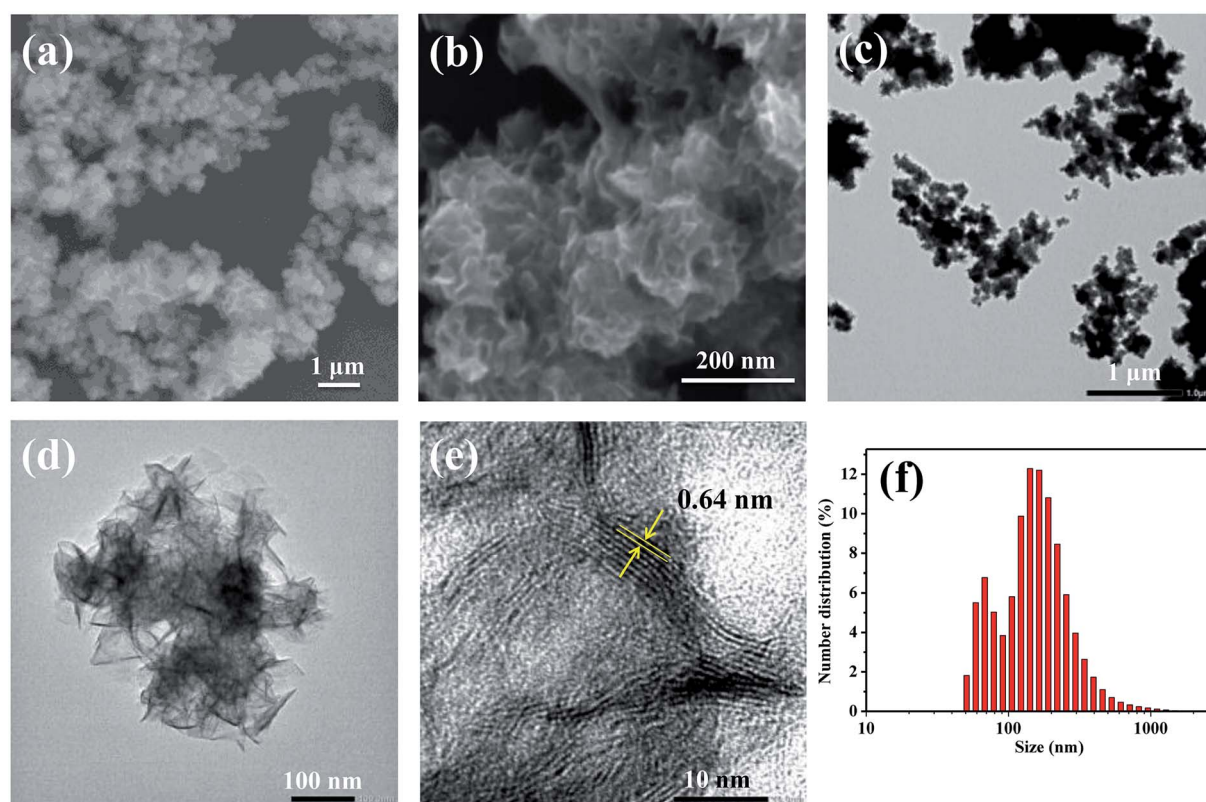


Fig. 1 (a and b) SEM images, (c–e) TEM images and (f) number distribution of carbon-doped MoSe<sub>2</sub>.



Dispersion method: 50 mL of isopropyl alcohol and 50 mL of distilled water were added in a beaker, and then the MoSe<sub>2</sub> powder was added into the isopropyl alcohol/distilled water mixture solution. Then the MoSe<sub>2</sub> nanoparticles were obtained with ultrasonic dispersion method, and the ultrasonic time was 4 h.

## 2.4 Characterization

Fourier transform infrared (FT-IR) was carried out between 400 and 4000 cm<sup>-1</sup> using a Bruker spectrophotometer (VERTEX70, Bruker, Germany). The carbon-doped MoSe<sub>2</sub> particles were investigated by X-ray photoelectron spectroscopy (XPS) analysis (Thermo Fisher ESCALAB Xi+, USA). X-ray diffraction (XRD) characterization was used to investigate the crystal phase structure patterns (D8 advance, Bruker, Germany). Scanning electron microscopy (SEM) was used to observe the MoSe<sub>2</sub> (SU3500, Techcomp, China). Energy dispersive spectrometer (EDS) was used to do the EDS elemental maps of the MoSe<sub>2</sub> on silicon wafer (OXFORD instruments, UK). Transmission electron microscope (TEM) (H-7650, HITACHI, Japan) was used to observe the MoSe<sub>2</sub>. The particle size and distribution were

determined by laser particle size distribution analyzer (ZSE, Malvern, UK). Thermo gravimetric analysis (TG) and differential scanning calorimetry (DSC) analyses were under an oxygen atmosphere from 30 to 1000 °C (STA449F5, NETZSCH, Germany).

## 2.5 BSA conjugation

Bovine serum albumin (BSA) can be used to bond with MoSe<sub>2</sub>. The BSA should be dissolved in phosphate-buffered saline [PBS: 150 mM NaCl, 1.9 mM NaH<sub>2</sub>PO<sub>4</sub>, 8.1 mM Na<sub>2</sub>HPO<sub>4</sub>, pH of 7.4] at a volume fraction of 1%. Then 1 mL of volume fraction of 1% BSA was added to 10 mL of MoSe<sub>2</sub> solution (6 µg mL<sup>-1</sup>) with gentle rocking for 12 h at room temperature. Subsequently, the response was ended by centrifugation at 10 000 rpm for 5 min to remove redundant BSA. Afterwards, the sediment was re-suspended by deionized water.

## 2.6 Fluorescence microscopy

Fluorescein isothiocyanate (FITC) was used to mark the BSA-coated MoSe<sub>2</sub> with green fluorescence. Briefly, FITC DMSO

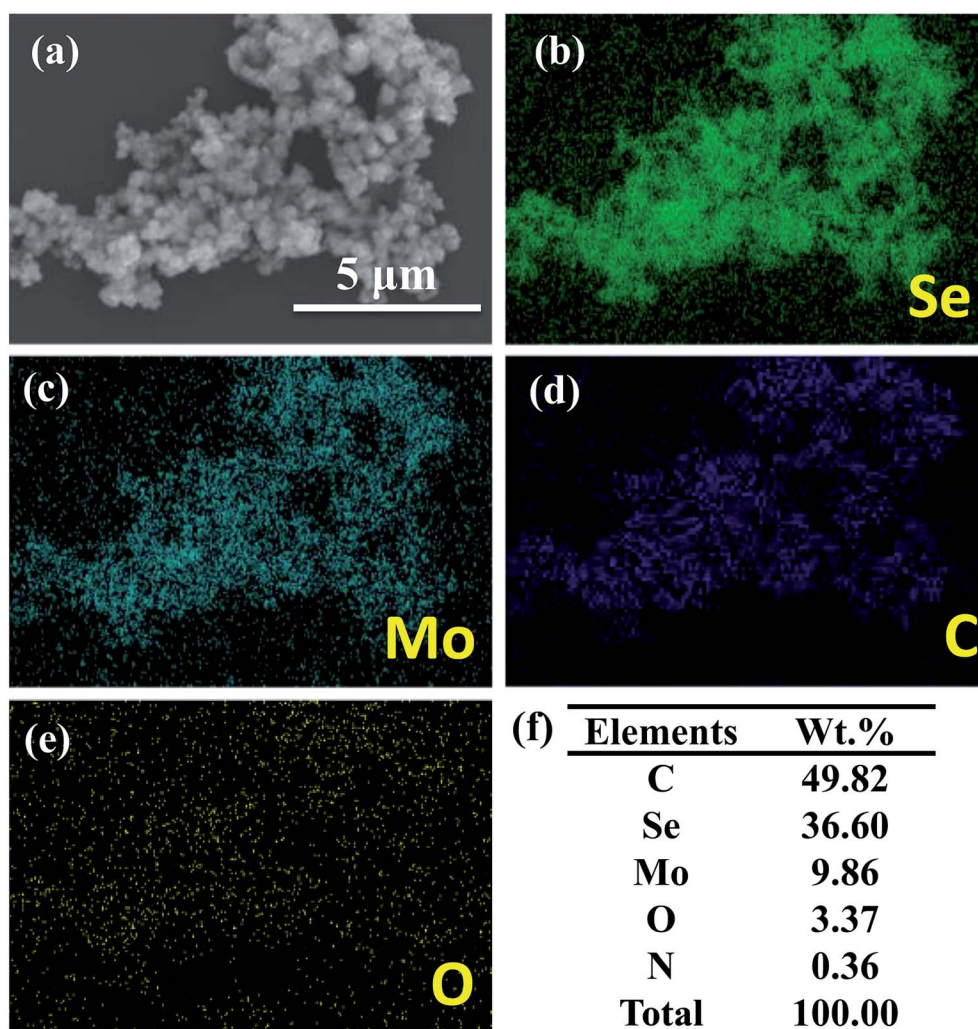


Fig. 2 (a) SEM image, (b–e) EDS elemental maps and (f) element wt% of carbon-doped MoSe<sub>2</sub>.





solution was added to BSA-coated MoSe<sub>2</sub> and the mixture was stirred for 4 h in darkness. Then the FITC-marked MoSe<sub>2</sub> was separated by centrifugation at 10 000 rpm for 5 min and washed three times with ice-cold PBS to remove the additional FITC. The 786-O, ACHN and HK-2 cells were seeded on slides and cultured for 24 h. Subsequently, the medium was removed and then the FITC-coated BSA-labeled MoSe<sub>2</sub> was added and the cells were incubated for another 4 h. After removing the medium, the cells were washed by cold PBS twice and cultured with 40, 6-diamidino-2-phenylindole (DAPI) dyed for 5 min at a concentration of 0.1 mg mL<sup>-1</sup>. The cells were measured by fluorescence microscope.

## 2.7 Flow cytometry assay

The renal carcinoma 786-O cells were treated by MoSe<sub>2</sub> at a concentration of 4 μg mL<sup>-1</sup> and 6 μg mL<sup>-1</sup> for 24 h. After being washed by PBS, the cells were gathered and dyed with FITC-conjugated Annexin V and propidium iodide (PI) by following the manufacturer's protocol. Afterwards, the apoptotic cells were analyzed according to flow cytometry (BD FACS can flow cytometer, BD Biosciences).

## 2.8 MTT method

The 786-O, ACHN and HK-2 (5 × 10<sup>3</sup> cells per well) were seeded onto 96-well plates and disposed with MoSe<sub>2</sub> (in the concentration of 0, 1 μg mL<sup>-1</sup>, 2 μg mL<sup>-1</sup>, 4 μg mL<sup>-1</sup>, 6 μg mL<sup>-1</sup>, 8 μg mL<sup>-1</sup>, 10 μg mL<sup>-1</sup>) for 24 h. After treatment, 20 μL MTT (3-(4,5-dimethyl-2-thiazolyl)-2,5-diphenyl-2H-tetrazolium bromide) was added to each well with 180 μL medium and incubated at 37 °C for 4 h. Then, dimethyl sulfoxide (DMSO) was added to dissolve the formazan crystals. The optical density of each well was examined at a wavelength of 490 nm according to a 96-well microplate reader (Bio-Rad, Hercules, CA, USA).

# 3 Results and discussion

## 3.1 SEM, TEM, number distribution and EDS analyses

Fig. 1 shows the morphology and physicochemical properties of the carbon-doped MoSe<sub>2</sub> nanoparticles. Fig. 1a shows the large scale morphologies of the synthesized MoSe<sub>2</sub> nanoparticles with SEM, and the high magnification SEM of carbon-doped MoSe<sub>2</sub> in Fig. 1b shows flower type. The TEM image of the Fig. 1c shows the large area of MoSe<sub>2</sub> nanoparticles. From the TEM images in Fig. 1d, it can be seen that the MoSe<sub>2</sub> is layer structure and shows flower morphology with a size of about 200 nm. According to the high magnification TEM of carbon-doped MoSe<sub>2</sub> in Fig. 1e, the lattice space of MoSe<sub>2</sub> is obviously. In addition, an interlayer distance of nearly 0.64 nm was examined, which matched the thickness of the single layer of Se-Mo-Se unit and the corresponding (002) plane.<sup>18</sup> It proved that the carbon-doped MoSe<sub>2</sub> had high crystallinity and extremely thin 2D flake structure with lattice space. Fig. 1f shows the number distribution of the MoSe<sub>2</sub> nanoparticles, and some of these particles are under 100 nm.

Fig. 2 shows the SEM image and EDS elemental maps of the MoSe<sub>2</sub> on silicon wafer. The EDS spectra detected Se, C, Mo, O

and N elements, and the EDS elemental maps as Fig. 2b–e shown. Furthermore, the Fig. 2f shows the MoSe<sub>2</sub> contained C (49.82 wt%), Se (36.60 wt%), Mo (9.86 wt%), O (3.37 wt%) and N (0.36 wt%), and C element is the most abundant element in MoSe<sub>2</sub>. The ethanol in the preparation processes with C element which caused the prepared MoSe<sub>2</sub> to contain C element. Moreover, the EDS analysis result shows that the weight ratios of Se and Mo are 36.60% and 9.86%. According to calculation, the atomic percent ratio of Se to Mo was 4.51 : 1, which further showed that the obtained product may consist of Se and MoSe<sub>2</sub>.

## 3.2 FT-IR, XRD, XPS and thermal analyses

The FT-IR spectrum of MoSe<sub>2</sub> is shown in Fig. 3a. The adsorption band from 1998 cm<sup>-1</sup> to 2662 cm<sup>-1</sup> is attributed to the stretching vibration of NH<sub>2</sub><sup>+</sup> and NH<sub>3</sub><sup>+</sup>. The adsorption peak at 1611 cm<sup>-1</sup> can be attributed to the variable angular vibration of NH<sub>2</sub> and NH<sub>2</sub><sup>+</sup>. And the adsorption band at 676 cm<sup>-1</sup> can be attributed to the C–OH out-plane bending from alcohols.<sup>19</sup> These carbon functional groups further proved that the MoSe<sub>2</sub>

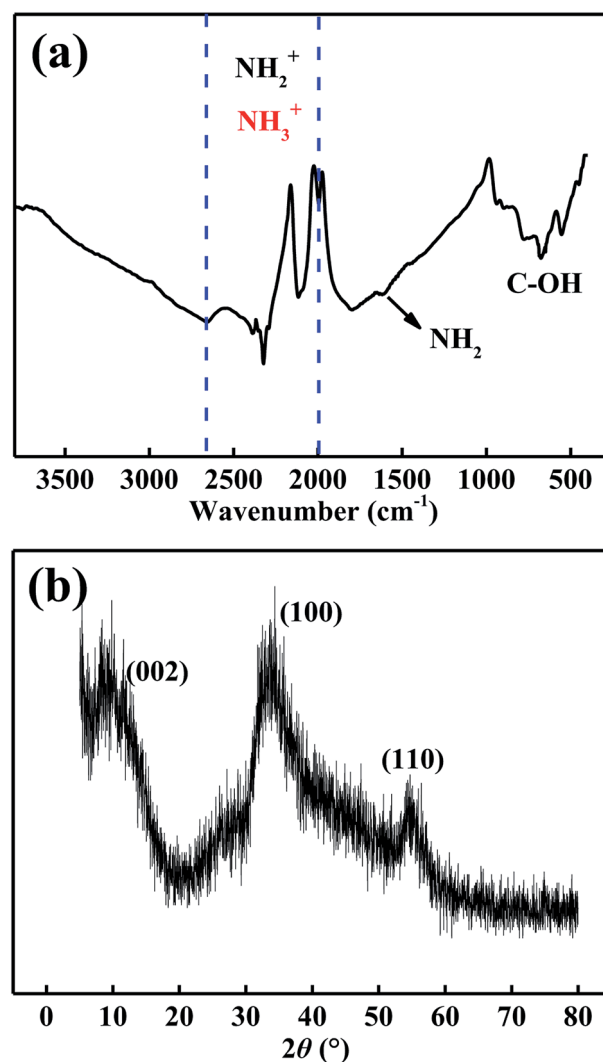


Fig. 3 (a) FT-IR spectrum and (b) XRD pattern of carbon-doped MoSe<sub>2</sub> nanoparticles.



particles contained C element after adding ethanol in preparation processes. As indicated in Fig. 3b, the characteristic diffraction peaks of the MoSe<sub>2</sub> nanoparticles on the XRD spectrum were agree with the standard pattern of the MoSe<sub>2</sub> crystal (JCPDS card no. 20-0757).<sup>12</sup> The XRD pattern of the MoSe<sub>2</sub> sample shows broad diffraction peaks, which reflects the nano size of products.<sup>20</sup> The above data revealed that the ethanol ultimately caused these MoSe<sub>2</sub> nanoparticles to contain C element, and the MoSe<sub>2</sub> nanoparticles contained C element also have classic MoSe<sub>2</sub> crystal.

XPS characterization was used to analysis the composition of elements and their chemical state. In Fig. 4, the atoms of C, Se, Mo, O and N were detected. In Fig. 4b, the fitting peaks mainly present in four groups: Se Auger, C 1s, C-OR and COOR 288.5 eV. The standard peak of C 1s is at 285.0 eV, and the fitting peak at 283.2 eV corresponding to C 1s because of the peak shifted 1.8 eV. In Fig. 4c, the Se 3d fitting peaks at 53.8 eV and 52.9 eV can be attributed to the Se 3d<sub>3/2</sub> and Se 3d<sub>5/2</sub>,<sup>20</sup> the two characteristic peaks of Se 3d<sub>5/2</sub> and Se 3d<sub>3/2</sub> reveal the existence state of Se<sup>2-</sup>.<sup>21</sup> And the standard peaks of Se 3d<sub>3/2</sub> and Se 3d<sub>5/2</sub> are at 55.7 and 54.9 eV, respectively, and the peaks shifted about 1.8 eV. In Fig. 4d, the fitting peaks of Mo 3d<sub>3/2</sub> and Mo 3d<sub>5/2</sub> are at 230.5 and 227.3 eV,<sup>22</sup> and the standard peaks are at 231.1 and 228.0 eV. The obtained XPS results were inconsistent with the standard values because of the peaks may shift. In Fig. 4e, the fitting peak at 532.6 eV shows the existence of C-OH because of the ethanol was added in the preparation process. Meanwhile, the peak at 529.5 eV can be attributed to the formation of MoO<sub>3</sub> on the surface of MoSe<sub>2</sub>.<sup>23</sup> And the small peaks of N 1s shows the MoSe<sub>2</sub> nanoparticles contain some residual N element (Fig. 4f).

Thermogravimetric analyzer was used to study the thermal stability of the carbon-doped MoSe<sub>2</sub> nanoparticles. As shown in

Fig. 5a, the weight loss about these films present different curves. The MoSe<sub>2</sub> nanoparticles will react with air, and the MoSe<sub>2</sub> nanoparticles have the weight increase before the temperature of 311 °C, and the weight of the sample increase was at about 6.65%. And the carbon-doped MoSe<sub>2</sub> nanoparticles have sharply weight loss in the temperature range of 338–437 °C, which can be attributed to the decomposition of the MoSe<sub>2</sub> nanoparticles. Then the MoSe<sub>2</sub> nanoparticles have little weight loss in the temperature range of 437–712 °C, and they have relatively steady weight loss in the temperature range of 712–908 °C. In addition, the weight of MoSe<sub>2</sub> nanoparticles become stable and shows a loss of 88.5% after 908 °C. DSC result indicated the total heat of melt, the endothermic peaks of MoSe<sub>2</sub> nanoparticles were at 283 °C and 709 °C (Fig. 5b). The data revealed that the two thermo-oxidative decomposition temperatures were at 283 °C and 709 °C. Compared with the 338 °C in TG (Fig. 5a), the weight increase revealed that the carbon-doped MoSe<sub>2</sub> nanoparticles were also reacted with air after 283 °C.

### 3.3 Cell evaluations

The cell viabilities of 786-O and ACHN cells were measured after being incubated with various concentrations of the carbon-doped MoSe<sub>2</sub> for 24 h. Fig. 6 shows that the carbon-doped MoSe<sub>2</sub> have good inhibited proliferation for renal cancer cells. Herein, it was found that the cell viabilities of 786-O were estimated to be less than 50% when the concentrations are up to 6 μg mL<sup>-1</sup> (Fig. 6a), and the cell viabilities of ACHN were estimated at about 50% when the concentrations are up to 4 μg mL<sup>-1</sup> (Fig. 6b).

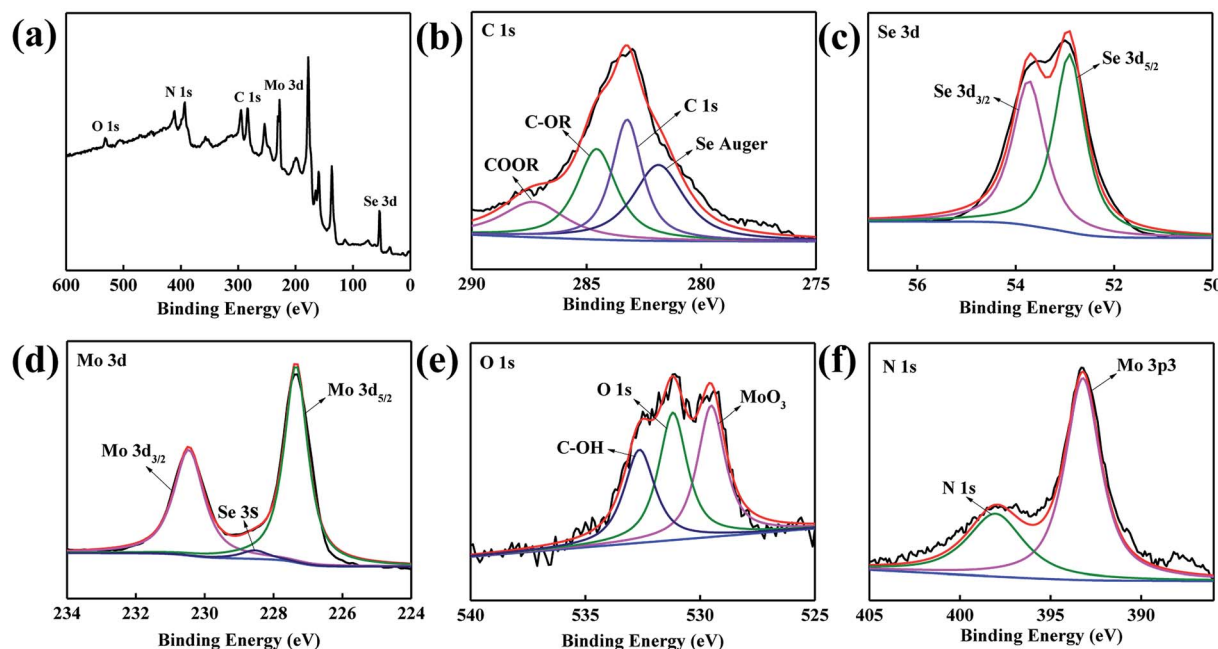


Fig. 4 (a) XPS spectrum of MoSe<sub>2</sub>, (b) high resolution XPS of C 1s, (c) high resolution XPS of Se 3d, (d) high resolution XPS of Mo 3d, (e) high resolution XPS of O 1s and (f) high resolution XPS of N 1s.



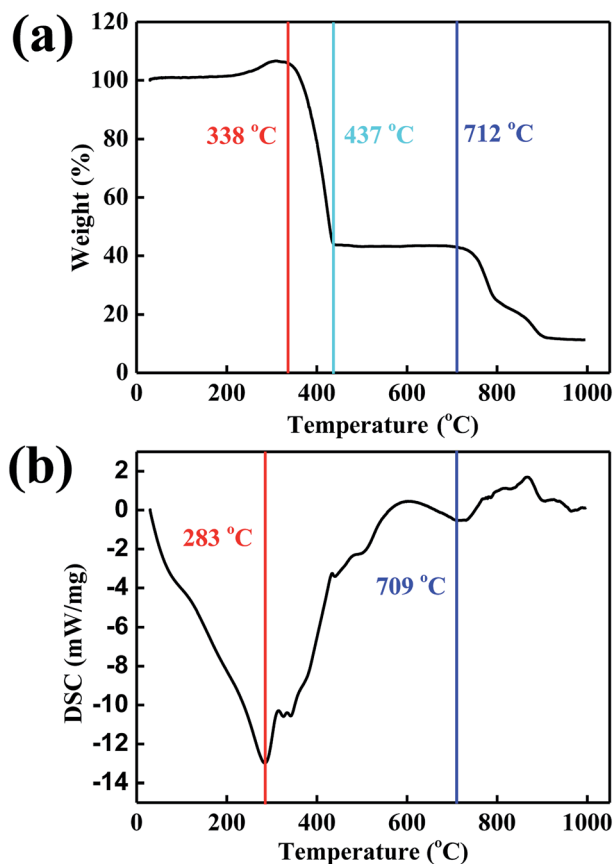


Fig. 5 (a) TG and (b) DSC curves of carbon-doped MoSe<sub>2</sub>.

Furthermore, the TUNEL assay was used to detect DNA fragmentation following the treatment of RCC cells with carbon-doped MoSe<sub>2</sub>. In Fig. 7, the FITC is activated after treating with carbon-doped MoSe<sub>2</sub>, including DNA damage, and is an essential regulator of apoptosis. Therefore, the effect of MoSe<sub>2</sub> treatment on FITC expression was analyzed. FITC expression was markedly upregulated in 786-O, ACHN and HK-2 cells after treating with carbon-doped MoSe<sub>2</sub> alone for 12 h. This experiment was used to quantify the difference in uptake in normal and tumor cells. As a result, there are less HK-2 cells

than tumor cells in fluorescence images, which indicated that the uptake ability of HK-2 cells for carbon-doped MoSe<sub>2</sub> particles was weaker than tumor cells.

To investigate whether the treatment with carbon-doped MoSe<sub>2</sub> could induce cell death in RCC cells, the 786-O renal cancer cells were treated with the agents. Apoptosis was detected using flow cytometry. As demonstrated in Fig. 8a, the 786-O cells are treated with alone carbon-doped MoSe<sub>2</sub>, the results exhibit increased apoptosis in RCC cells. In Fig. 8b, the percentage of apoptotic 786-O cells following carbon-doped MoSe<sub>2</sub> treatment were 18.2% (4  $\mu\text{g mL}^{-1}$ ) and 20.5% (6  $\mu\text{g mL}^{-1}$ ), which had significantly increased compared with medium and control treatment.

### 3.4 Bio-TEM analyses

Bio-TEM image in Fig. 9a shows the MoSe<sub>2</sub> particles in the 786-O cell, and the 786-O cell can uptake the big particles (above 1  $\mu\text{m}$ ). Moreover, Fig. 9b shows the high-magnification image and it further confirms that these MoSe<sub>2</sub> particles are easy to reunite. All these results indicate that the tumor cells have high cellular uptake efficiency for MoSe<sub>2</sub>, possibly due to the albumin receptor-mediated endocytosis pathway in the cells.<sup>13,14,24–26</sup> And the reason of apoptosis may be related to the autophagic lysosome, because this material can combine with the lysosome. As a result, the carbon-doped MoSe<sub>2</sub> particles could enter the 786-O cells and inhibited the proliferation.

### 3.5 Relevant mechanisms

Considering that the ideal agent should have good biocompatibility for biomedical field applications, the cytotoxicity of the carbon-doped MoSe<sub>2</sub> was evaluated. Herein, the cell viabilities of HK-2 cells were measured after being incubated with various concentrations of the MoSe<sub>2</sub> for 24 h. It was found that no obvious toxicity was observed for these cells. The cell viabilities decrease with the concentration increasing, and all the results estimate to be greater than 90% (Fig. 10a). Because the normal cells have weaker cellular uptake efficiency than tumor cells, and the uptake ability may cause small particles to enter the cells, but the big MoSe<sub>2</sub> particles can't enter the HK-2

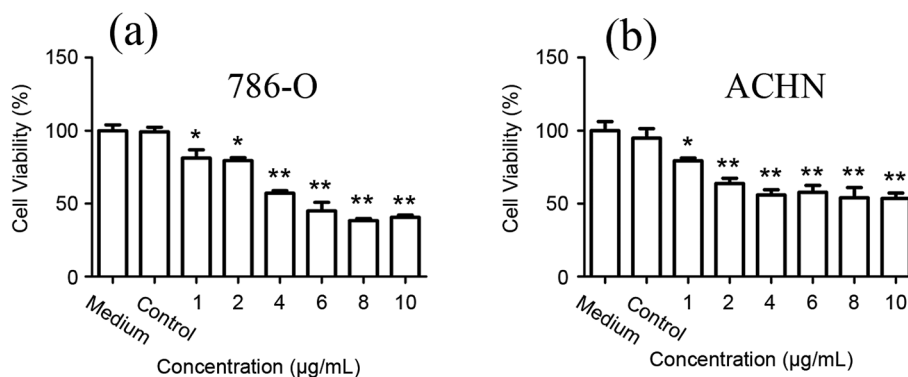


Fig. 6 MoSe<sub>2</sub> inhibited proliferation of renal cancer cells (a) 786-O and (b) ACHN were treated with different concentration of MoSe<sub>2</sub> or DMSO (control) for 24 h, and MTT assay was applied to test cell viability. Results are shown as the mean  $\pm$  SD. \* $p$  < 0.05, \*\* $p$  < 0.01.



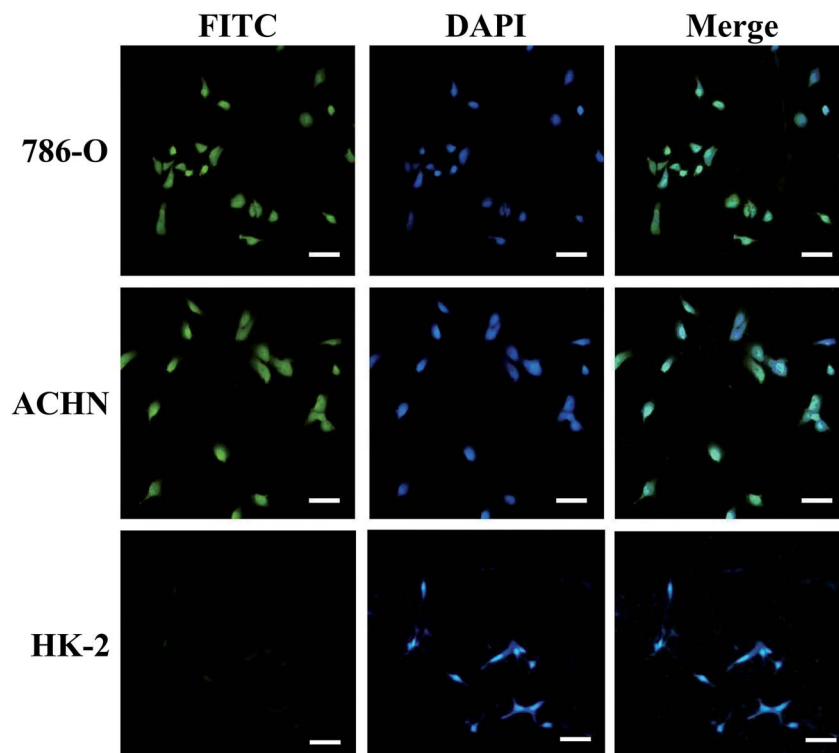


Fig. 7 Fluorescence images of 786-O, ACHN and HK-2 cells incubated with the BSA-coated MoSe<sub>2</sub> for 12 h. All the MoSe<sub>2</sub> were labeled with FITC. The cell nuclei are stained with DAPI (blue) and the scale bar is 50  $\mu$ m.

cells as Fig. 10b shown. So, less MoSe<sub>2</sub> particles can't inhibit the proliferation for HK-2 cells.

Furthermore, normal MoSe<sub>2</sub> particles have poor suspension property and they are easy to precipitate because of particles aggregation in water. But the Fig. 10c shows that the carbon-doped MoSe<sub>2</sub> particles have good suspension performances.

The FT-IR and XPS show that the carbon-doped MoSe<sub>2</sub> particles have C–OH, COOR, C–OR and NH<sub>2</sub>, and these particles will have hydrogen bond effect in aqueous solution.<sup>27–29</sup> As a result, these carbon-doped MoSe<sub>2</sub> nanoparticles will bonded with each other *via* hydrogen bond effect to form big particles. So, these carbon-doped MoSe<sub>2</sub> particles appeared precipitation phenomenon

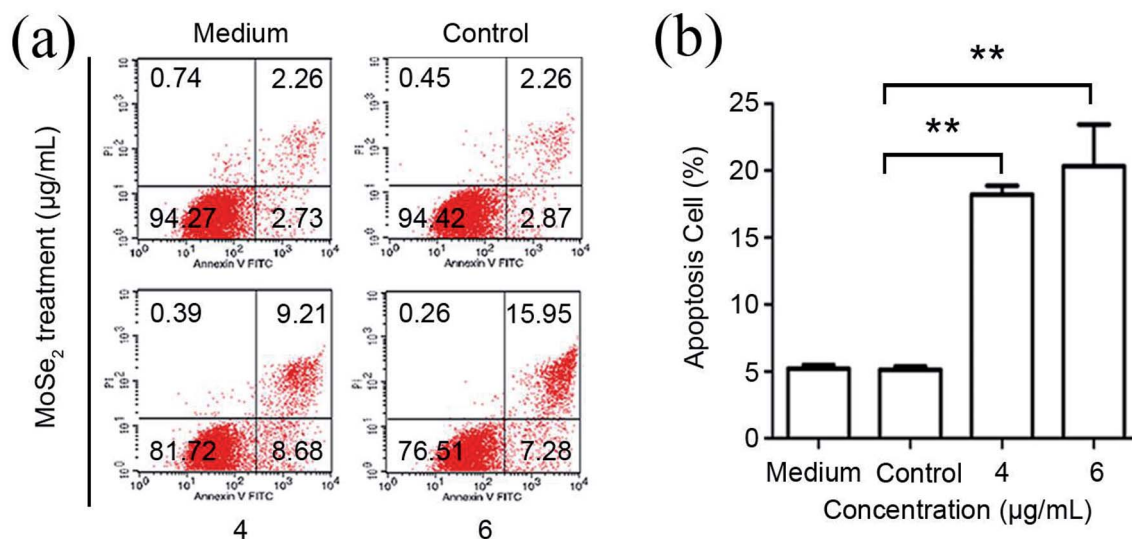


Fig. 8 MoSe<sub>2</sub> promoted apoptosis of 786-O cells. (a) Flow cytometry analysis and (b) statistical analysis to detect the apoptotic effect of MoSe<sub>2</sub> on 786-O cells. After treatment with MoSe<sub>2</sub> for 24 h, 786-O cells were harvested and stained with annexin-V/propidium iodide (PI), and followed by FACS analysis as mentioned above. Results are shown as the mean  $\pm$  SD. \*\* $p$  < 0.01.





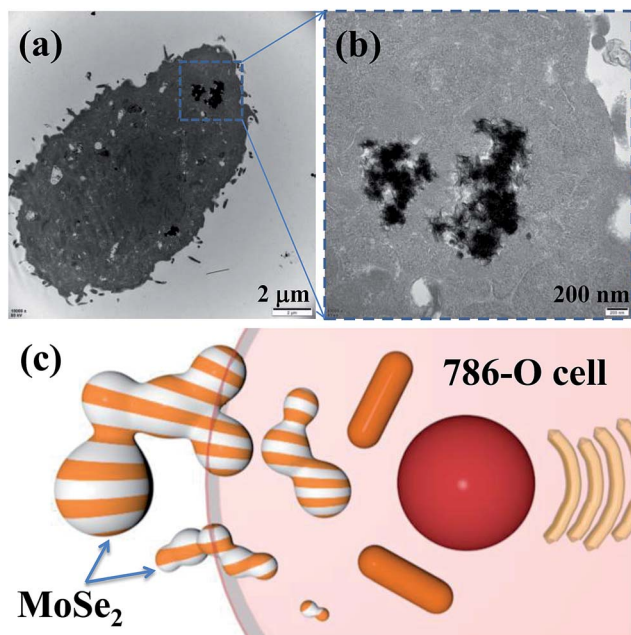


Fig. 9 (a and b) Bio-TEM images of the MoSe<sub>2</sub> treated 786-O cell, and (c) schematic illustration of MoSe<sub>2</sub> particles in 786-O cell.

during 6 h because of the formation of big MoSe<sub>2</sub> particles. And in the next days, the precipitation speed was slow, and then the speed became relatively steady after 3 days. It is because the MoSe<sub>2</sub> nanoparticles formed big particles, and these big

particles will further crosslink with each other *via* hydrogen bonds to form a bonded network structure. At this point, the hydrogen bond effect is beneficial to suspend for the carbon-doped MoSe<sub>2</sub> particles.

The tumor cells have higher uptake ability than HK-2 cells, the carbon-doped MoSe<sub>2</sub> particles can be absorbed by tumor cells and then cause apoptosis. The reason of apoptosis may be related to the autophagic lysosome, because this material can combine with the lysosome. In conclusion, the MoSe<sub>2</sub> nanoparticles reunited to form bigger particles, and the HK-2 cells could not uptake these big particles which caused the HK-2 cells to have high viabilities.

## 4 Conclusions

This study prepared carbon-doped MoSe<sub>2</sub> nanoparticles, and the EDS, FT-IR, XPS, TG and DSC proved that the MoSe<sub>2</sub> nanoparticles contained carbon compound. And the fluorescence microscopy, flow cytometry assay and MTT results revealed that the carbon-doped MoSe<sub>2</sub> nanoparticles have significantly anti-cancer effect, and the 786-O and ACHN cells were markedly reduced after MoSe<sub>2</sub> treating. Meanwhile, the carbon-doped MoSe<sub>2</sub> nanoparticles with the high viability for KH-2 cells *in vitro* (above 90%), which indicated that these carbon-doped MoSe<sub>2</sub> nanoparticles with minimal toxicity. The mechanism analyses revealed that the carbon-doped MoSe<sub>2</sub> particles have good suspension property in aqueous solution, and then the aggregation effect caused the MoSe<sub>2</sub> particles to

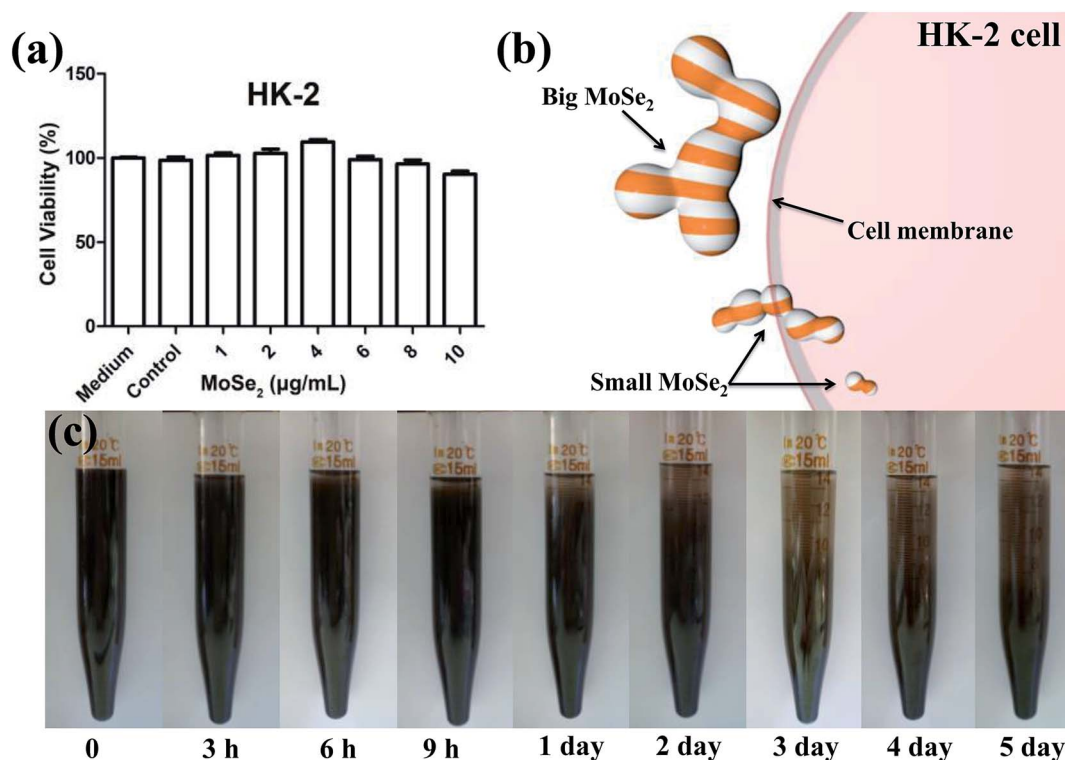


Fig. 10 (a) Viabilities of HK-2 cells incubated with the MoSe<sub>2</sub> at different concentrations for 24 h, (b) schematic illustration of MoSe<sub>2</sub> particles in 786-O cell, and (c) suspension performances of the MoSe<sub>2</sub> particles in distilled water.





become bigger. The tumor cells have higher uptake ability than HK-2 cells, which finally caused the KH-2 cells to have higher viability in carbon-doped MoSe<sub>2</sub> concentration. These carbon-doped MoSe<sub>2</sub> particles have obviously anti-cancer effect to 786-O and ACHN cells and with good biocompatibility to KH-2 cells, which suggested that these materials may be a potential therapeutic candidate against RCC.

## Author contributions

All authors discussed the results and commented on the manuscript. L. G. and Y. Z. F. contributed equally to this work and should be considered co-first authors.

## Conflicts of interest

There is no conflict between the authors, and there are no conflicts of interest.

## Acknowledgements

This work is supported by National Natural Science Foundation of China (No. 81672538).

## References

- 1 C. Liang, Y. Chao, S. Sida, Y. Xuan, G. Hua, Y. Kai and L. Zhuang, *ACS Nano*, 2015, **9**, 11090–11101.
- 2 K. D. Miller, R. L. Siegel, C. C. Lin, A. B. Mariotto, J. L. Kramer, J. H. Rowland, K. D. Stein, R. Alteri and A. Jemal, *Ca-Cancer J. Clin.*, 2016, **66**, 271–289.
- 3 P. Camparo, *Diagn. Interv. Imaging*, 2012, **93**, 221–231.
- 4 H. T. Cohen and F. J. McGovern, *N. Engl. J. Med.*, 2005, **353**, 2477.
- 5 S. Duensing and M. Hohenfellner, *Lancet*, 2016, **387**, 1973–1974.
- 6 I. J. Frew and H. Moch, *Annu. Rev. Pathol.*, 2015, **10**, 263–289.
- 7 H. Axelson and M. E. Johansson, *Semin. Canc. Biol.*, 2013, **23**, 56–61.
- 8 C. Manish, L. Zhongfan and Z. Hua, *Chem. Soc. Rev.*, 2015, **44**, 2584–2586.
- 9 Y. Lichun, W. Sinong, M. Jianjiang, D. Junwen, G. Qingsheng, T. Yi and O. G. Schmidt, *Adv. Mater.*, 2013, **25**, 1180–1184.
- 10 B. Mao, T. Bao, J. Yu, L. Zheng, J. Qin, W. Yin and M. Cao, *Nano Res.*, 2017, **10**, 2667–2682.
- 11 W. Z. Teo, E. L. Chng, Z. Sofer and M. Pumera, *Chemistry*, 2014, **20**, 9627–9632.
- 12 J. Pan, X. Zhu, X. Chen, Y. Zhao and J. Liu, *Biomater. Sci.*, 2018, **6**, 372–387.
- 13 C. Zhong, X. Zhao, L. Wang, Y. Li and Y. Zhao, *RSC Adv.*, 2017, **7**, 7382–7391.
- 14 J. Chen, X. Li, X. Liu, H. Yan, Z. Xie, Z. Sheng, X. Gong, L. Wang, X. Liu, P. Zhang, H. Zheng, L. Song and C. Liu, *Biomater. Sci.*, 2018, **6**, 1503–1516.
- 15 L. Yuwen, J. Zhou, Y. Zhang, Q. Zhang, J. Shan, Z. Luo, L. Weng, Z. Teng and L. Wang, *Nanoscale*, 2015, **8**, 2720.
- 16 Z. Lei, W. Zhu, S. Xu, J. Ding, J. Wan and P. Wu, *ACS Appl. Mater. Interfaces*, 2016, **8**, 20900–20908.
- 17 C. Wang, J. Bai, Y. Liu, X. Jia and X. Jiang, *ACS Biomater. Sci. Eng.*, 2016, **2**, 2011–2017.
- 18 J. Huang, B. Jin, H. Liu, X. Li, Q. Zhang, S. Chu, R. Peng and S. Chu, *J. Mater. Chem. A*, 2018, **6**, 11424–11434.
- 19 S. wen, *Fourier transform infrared spectrometry*, Chemical Industry Press, 2010.
- 20 H. Tang, K. Dou, C.-C. Kaun, Q. Kuang and S. Yang, *J. Mater. Chem. A*, 2014, **2**, 360–364.
- 21 Z. Lei, S. Xu and P. Wu, *Phys. Chem. Chem. Phys.*, 2015, **18**, 70–74.
- 22 H. Wang, D. Kong, P. Johanes, J. J. Cha, G. Zheng, K. Yan, N. Liu and Y. Cui, *Nano Lett.*, 2013, **13**, 3426–3433.
- 23 N. Xue and P. Diao, *J. Phys. Chem. C*, 2017, **121**, 14413–14425.
- 24 S. Baghaie, M. T. Khorasani, A. Zarrabi and J. Moshtaghian, *J. Biomater. Sci. Polym. Ed.*, 2017, **28**, 2220–2241.
- 25 F. Zou, R. Li, J. Jiang, X. Mo, G. Gu, Z. Guo and Z. Chen, *J. Biomater. Sci. Polym. Ed.*, 2017, **28**, 2255–2270.
- 26 E. Dalton and M. N. Collins, *J. Appl. Crystallogr.*, 2014, **47**, 847–851.
- 27 H. Lu, L. Lv, J. Ma, W. Ban, S. Ren, G. Dong, J. Li and X. Dang, *J. Mech. Behav. Biomed. Mater.*, 2018, **88**, 261–269.
- 28 H. Lu, S. Ren, P. Zhang, J. Guo, J. Li and G. Dong, *RSC Adv.*, 2017, **7**, 21600–21606.
- 29 H. Lu, S. Ren, J. Guo, Y. Li, J. Li and G. Dong, *Mater. Sci. Eng., C*, 2017, **78**, 239–245.

